Microstructure and wear resistance of (Nb,Ti)C carbide reinforced Fe matrix coating with different Ti contents and interfacial properties of (Nb,Ti)C/α-Fe

C. Zhao[a], X.Xing[a,b], J. Guo[c], Z. Shi[a], Y. Zhou[a,b] X.J. Ren[d], Q. Yang[a]

[a] State Key Laboratory of Metastable Materials Science & Technology, Yanshan University, Qinhuangdao 066004, PR China

[b] College of Mechanical Engineering, Yanshan University, Qinhuangdao 066004, PR China

[c] College of Metallurgy and Energy, North China University of Science and Technology, Hebei Key Laboratory of Modern Metallurgy Technology, Tangshan 063009, China

[d] School of Engineering, Liverpool John Moores University, Liverpool L3 3AF, UK

Abstrtact
In this work, the (Nb,Ti)C reinforced Fe matrix coatings were prepared by gas metal arc welding (GMAW) hardfacing technology. The microstructure, hardness and wear resistance of (Nb,Ti)C reinforced coatings with different Ti contents were investigated by experiments. The interfacial properties of (Nb,Ti)C/α-Fe interfaces were calculated by first principles method based on density functional theory (DFT). The experiment results show that as the Ti content in the coating changes from 0.15 to 0.41 wt%, the average diameter of NbC primary carbide grains decreases from 3.2 μm to 1.7 μm and their amount increase from 0.35 to 0.51 μm−2. The coating with 0.15 wt% Ti performs the lowest wear loss, which is 0.47 g/N ∗ cm2. From the calculated results, the interfacial combination between carbide and matrix are improved after Ti addition. The adhesion work of (Nb,Ti)C/Fe interfaces show the following order: CNb-Fe < NbC-Fe < CTiNb-Fe < CNbTi-Fe < NbTiCFe < TiNbC-Fe. In CTiNb-Fe, CNbTi-Fe and CNb-Fe surfaces, weak Fe-M covalent bonds are formed at the interfaces. In NbC-Fe, NbTiC-Fe and TiNbC-Fe surfaces, strong FeeC and M-C covalent bond can be found at (Nb,Ti)C/α-Fe interfaces, besides, FeeC ionic bonds are also formed.

Keywords: (Nb,Ti)C carbide, Microstructure, Wear resistance, Interfacial combination, Bonding structure

1. Introduction

Niobium carbide reinforced Fe-based composite coatings have been widely applied in materials strengthening, due to their high strength, excellent thermal stability, outstanding wear resistance and price advantage[1,2]. And it has been found that the performance of coating with multiple carbides is better than that with single carbide [3–6]. Li et al. [7] research the formation mechanism of (Ti, Nb)C carbide in (Ti, Nb)C reinforced Fe-based composite coatings with different Ti/Nbatomic ratio. And they found that the wear resistance of coating withTi/Nb=1 is the best. It can be learnt from our previous work [8,9]that, element Ti can improve the hardness of carbide and decrease the misfit between carbide and matrix. Besides, it can also change the morphology of carbide by changing the precipitation order of carbide and matrix. The morphology [10,11], size and distribution [10,14]changes of carbide are complex but important factors, which can strongly affect the wear resistance of carbide-reinforced composite coatings [12,13]. In (Ti, Nb)C reinforced Fe-based composite coatings, the morphology and size of carbide will be changed with different Ti contents. However, few investigations on morphology evolution of Nb Carbide affected by different Ti contents were reported.

The combination of carbide with matrix is another important factor affecting the wear resistance of the coating. The strain energy of NbC/Fe interface is high and its interfacial energy is negative [6,15,16], which can partly reflect the dissatisfactory combination between NbC and Fe matrix. TiC has been reported to perform good combination with Fe [17,18], therefore the introduction of element Ti into carbide may perform positive effects on interfacial combination, which need to be investigated. However, it is very difficult to investigate the inner effect of element Ti on the interfacial combination between carbide an matrix by experiments. First-principles calculation has been widely used to study the interfacial bonding structure of materials. Fan et al. [19] research bonding characteristic and electronic property of TiC (111)/TiN (111) interface and indicated that, the bonding nature at the interface is extremely similar to that in bulk materials with both ionic and covalent characteristics. Wang et al. [20] investigated the misfit dislocation for Pt/SiC(111) interface fracture and found that the single Pt layer left on the SiC(111) surface with a mixture of covalent and ionic bonds. Yang et al. [21] studied interfacial properties of Ag (111)/SiC (111) interface and Ag (111)/TiC (111) interfaces and found that SiC ceramic improves the wettability of Ag-Cu-Ti filler metal on SiC ceramic. The interfacial combination between carbide and matrix can be investigated by adhesion work and bonding structures at the interfaces. It seems that, the interfacial combination of carbide and matrix with different Ti content can be investigated by first-principles calculations.

In this work, the morphology and microstructure changes of the carbides with different Ti contents were analyzed. The hardness and wear resistance of coatings were evaluated. Subsequently, the interfacial adhesion work, interfacial atomic structure and bonding structures of (Nb,Ti)C/α-Fe interfaces were calculated to analysis the wear resistance results.

2. Experimental methods and computational details

2.1. Experimental methods

The (Nb,Ti)C carbide reinforced Fe matrix composites coatings were prepared by gas metal arc welding (GMAW) hardfacing technology. The flux-cored wires were deposited on Q235 low-carbon steel plates. The flux-cored wire was covered by low-carbon steel strip of H08A, with graphite,ferrochromium, ferrovanadium, ferrotitanium, ferromanganese, ferroniobium and ferrosilicon powder in it. The details of fluxcored

wire manufacturing and hardfacing process were based on our previous work [22]. The compositions of the coatings with different Ti contents were test by Advant/P-381 spectrograph and CS-8800 sulfur carbon analyzer, and the compositions are listed in Table 1.

The Rigaku D/Max-2500/PC X-ray diffraction (XRD) with CuKa operating at 40 kV was used to identify the phases in the coatings. The hardfacing specimens were etched with 4% nitric acid alcohol. The microstructure of coatings and worn surfaces were performed with a HITACHI S-4800 scanning electron microscope (FE-SEM). 5 SEM images of 1 k magnification were selected to measure the amount and size of primary carbide by image measure analysis software. The microstructures of primary carbide and eutectic carbide were performed with a JEM-2100 transmission electron microscopy (TEM) equipped with an energy-dispersive spectroscopy (EDS).

The abrasive belt type wear testing machine in dry friction with SiC of 40 mesh abrasive material was used to evaluate the wear resistance of coatings. The specimen size, wear velocity and loading force were 20mm×10mm×15 mm, 1.8×104 mm/min and 100 g, respectively.The wear weightlessness was obtained by the averages of six measurements. The hardness was obtained by the averages of ten measurements
measured using a HR-105A Rockwell hardness tester.

2.2. Computational details

The interfacial properties of (Nb,Ti)C/α-Fe interfaces were calculated by First-principles method based on density functional theory (DFT) with ultrasoft pseudopotentials [23,24]. The calculations were performed by using CASTEP code (Cambridge Sequential Total Energy Package) [25]. Generalized gradient approximation (GGA) with Perdew-Burke-Ernzerhof (PBE) functional was employed as the exchange- correlation functional [26]. Based on the convergence tests, the plane–wave cutoff energy [23] was set at 380 eV and the Brillouin zone sampling was set at 8×8×1 Monkhorst-Pack mesh for the (Nb,Ti)C/ Fe interface calculation [27]. And the 13 layers (Nb,Ti)C and 5 layers Fe surfaces are selected. A 12 Å vacuum space along the c-axis was used to eliminate the long interactions from periodic boundary condition calculation, during interface calculation. The Broyden-FletcherGoldfarb- Shanno optimization method was used to converge the energy [28]. For the convergence tolerances, the energy of 1×10−5 eV/ atom, the maximum force of 0.01 eV/Å and maximum displacement of 1×10−3 Å were set, respectively.

3. Morphology, hardness and wear resistance of coatings

3.1. Microstructures with different Ti contents

Fig. 1 is the XRD results of the coatings. From Fig. 1, all the coatings are consist of α-Fe, γ-Fe and MC type carbide. Besides, the (111) and (200) peak shift of MC carbides can be observed with the increase of Ti content, which indicates that the lattice parameter of the carbide is reduced. From our previous work [29], the microstructures of the coatings are constituted of martensite (α-Fe), a small amount of retained austenite (γ-Fe) and (Nb,Ti)C carbide. The morphology of coatings is shown in Fig. 2, and it can be found that the morphology of the carbides in the coatings are changed significantly with the increase of Ti contents. The carbides in Ti-0 coating are almost all in form of eutectic carbide. However, in the Ti-1, Ti-2 and Ti-3 coatings, granular primary carbides began to appear. The amount of primary carbide is increased and size of carbides is decreased. The statistical results of the primary carbide in Ti-1, Ti-2 and Ti-3 coatings are shown in Fig. 3. From it, the average diameter of primary carbide in the Ti-1, Ti-2 and Ti-3 coatings are about 3.2 μm, 2.3 μm and 1.7 μm, respectively. The average amount of primary carbide in the coatings is about 0.35, 0.48 and 0.53 per square micron, respectively. The Gibbs free energy of TiC is lower than that of NbC [6,30], and the element Ti is believed to improve the precipitation ability of primary NbC carbide [8], therefore the amount of primary carbides are increased with the increase of Ti contents. However, the

increase in the amount of primary carbides will decrease the content of elements Nb, Ti and C in the molten pool, which may be the reason why the size of carbides are decreased with the increase of Ti content.

Fig. 4 is the TEM image and selected area electron diffraction pattern of primary carbide and eutectic carbide of T-3 coating. From it, the primary carbide and eutectic carbide are all face centered cubic structures with the zone axis $[0\bar{1}1]$ and $[\bar{2}11]$, respectively. The EDS element analysis results of primary carbide and eutectic carbide are listed in Table 2. The two types of carbides are mainly composed of Nb, Ti and C. And the Ti content in primary carbide is higher than that in eutectic carbide.

3.2. Hardness and wear resistance of the coatings

The hardness and wear weightlessness of the coatings with different Ti contents are shown in Fig. 5. From it, the hardness of Ti-0 coating is about HRC56, and the hardness of coatings are slightly decreased with the increase of Ti content, which may relate to the decrease of C content of the matrix. However, the wear loss of the coatings shows different tendency with the increase of Ti content. The wear loss of Ti-1 coating is the lowest, which is 0.47 g/N ∗cm2. The wear loss of Ti-2 and Ti-3
coatings are increased with the increase of Ti content, however, they are significantly lower than that of Ti-0 coating. In order to analyze the wear resistance tendency of coatings, the morphology of worn surfaces were analyzed, which are shown in Fig. 6. The deep furrows can be observed in the Ti-0 coating. The NbC and Fe interface shows negative interfacial energy and high strain energy, which means the combination of NbC with the Fe matrix is poor [15,31]. Therefore the deep furrows are believed to be caused by the loose and slide of the eutectic NbC carbides. In the Ti-1 coating, the broken carbides can be observed, which act as the reinforcements to block the abrasion paths. The sliding carbides have been observed in smaller carbides reinforced Ti-2 and Ti-3 coatings, in which, some of the smaller carbides did not function well to prevent the abrasion path, but slide with the sliding path together.

4. Interfacial properties of (Nb,Ti)C/α-Fe interfaces

The combination of carbide with matrix is also an important factor affecting the wear resistance of the coating. However, it is very difficult to make it clear by experiments for the element content changes and experimental sensitivity. First principles calculation has performed well for interfacial properties investigation. Therefore, the interfacial properties of (Nb,Ti)C/α-Fe interfaces were investigated to achieve a better understand of wear results.

4.1. Interface model and adhesion work

Based on our previous work, the matrix in the coatings is the martensite (α-Fe), and the carbide are mainly connected with α-Fe, therefore, (Nb,Ti)C/α-Fe interface was selected in this work. The element compositions of (Nb,Ti)C carbide have been reported [7,8], in which, element Ti is rich in the core area of the carbide and element Nb is rich in the part of carbide near the matrix. Therefore, the combination of (Nb,Ti)C with α-Fe was calculated using the interface model of Nb0.75Ti0.25C with α-Fe. The crystallographic relationship of the interface models were based on the Baker-Nutting relationship ((100)a-Fe∥(100)(Nb,Ti)C,[010]a-Fe∥[011](Nb,Ti)C) [32]. In the interface models, metal or carbon atoms in carbides can be put above on the Fe

atoms, which are defined as M-termination and C-termination interfaces. The M-termination and C-termination interfaces can be further divided based on the position of Ti atoms, and the details of (Nb,Ti)C and α-Fe interface models are shown in Fig. 7.

The adhesion work (Wad) of (Nb,Ti)C/Fe interfaces, which can reflect the interface stability, can be obtained as follows [33,34]:

$$W_{ad} = (E_{Fe} + E_{(Nb,Ti)C} - E_{Fe/(Nb,Ti)C})/A \quad (1)$$

where $E_{(Nb,Ti)C}$ and E_{Fe} denote the energies of 13 layers (Nb,Ti)C and 5 layers Fe surfaces relaxed, respectively; $E_{Fe/(Nb,Ti)C}$ is the total energy of the Fe/(Nb,Ti)C interfaces; A is the interface area. The calculated results of the W_{ad} are listed in Table.3. From Table 3, the W_{ad} of C-termination interfaces are larger than those of M termination interfaces, which indicates that the C-termination interface is more stable than M-termination one. After the introduction of Ti element, the Wad is also increased compared with pure NbeFe interfaces, which indicates that the introduction of Ti element increases the stability of the interface. In the M termination interface, the stability of the CNbTi-Fe model is higher than that of CTiNb-Fe one. In the C termination interface, the stability of the TiNbC-Fe model is higher than
that of the NbTiC-Fe one. The interfaces show the following stability order: CNb-Fe < NbC-Fe < CTiNb-Fe < CNbTi-Fe < NbTiC-Fe < TiNbC-Fe. The interface distance d_0 and the secondary neighbor atom distance d1 of M-termination and C-termination interfaces are shown in Fig. 8. The calculated results of d_0 and d_1 are listed in Table.3. The d_0 of the C-termination interfaces is smaller than that of M-termination ones and CNbTi-Fe interface shows the largest d_0. Besides, the d_1 of the C-termination interfaces are closed to d_0 of M-termination interfaces, which indicate that there may be Fe-M interactions except for Fe-C interactions in the C-termination interfaces.

4.2. Bonding structures between (Nb,Ti)C carbide and α-Fe matrix

Partial electronic density of states (PDOS) of different interface models is shown in Fig. 9. The shape of d orbital peaks of Fe atoms at the interface are strongly affected by element Ti. The PDOS of Fe atom at the Fermi level (E_F) are larger than 0 in all interfaces, and the PDOS of M-termination interfaces are larger than that of C-termination ones, which indicates that the metallic character of Fe atom at M-termination interfaces are stronger than that of C-termination ones. In C- termination interfaces, orbital hybridization of Fe-3d and C-2p orbits can be found, especially in NbTiC-Fe and TiNbC-Fe interfaces, which indicates the formation of FeeC covalent bonds.

The electrons transfer and distribution of the atom at interfaces can be obtained from charge densities and charge density differences. The charge density can be get directly from calculation. The charge density difference ΔρFe/(Nb,Ti)C can be obtained as follows [17,24]:

$$\Delta\rho_{\alpha\text{-}Fe/(Nb,Ti)C} = \rho_{Total} - \rho_{\alpha\text{-}Fe} - \rho_{(Nb,Ti)C} \quad (2)$$

where ρ_{Total} is the total charge density of the α-Fe/(Nb,Ti)C interfaces; $\rho_{\alpha\text{-}Fe}$ and $\rho_{(Nb,Ti)C}$ are the charge densities of the α-Fe and (Nb,Ti)C relaxed isolated slabs, respectively.

The charge density difference and charge density plots of M-termination and C-termination interfaces along plane ($1\bar{1}0$) are shown in Fig. 10 and Fig. 11. From Fig. 10(a), the Fe atoms at the interface obtained electrons compared with the ones at the inner Fe layer. Besides, the electrons transfer at the inner Fe layer can also be found. From Fig. 10(b), there are weak electrons distribution between Fe and Nb atoms at the interfaces. From the calculated bond population listed in Table 4, the Fe-Nb bond populations of CNb-Fe and CNbTi-Fe interfaces are negative values, which indicate the formation of unstable antibonds. In the CNbTi-Fe and CTiNb-Fe interfaces, weak covalent bonds are formed from the Fe and Ti atoms, and the Fe and Nb atoms, respectively. From Fig. 11(a), the Fe atoms at the interface lose electrons compared with the ones at the inner Fe layer. And the electron transfer at the inner Fe layer in C-termination interface models is weaker than that of M-termination interface models. From Fig. 11(b), the electrons with directional spatial distribution can be observed between Fe and C atoms, which indicate the formation of strong Fe-C covalent bonds. The bond population of C-termination interfaces shows that the Fe-C covalent bonds in NbTiC-Fe and TiNbC-Fe interfaces are stronger than that of NbC-Fe interface. There are also Fe-M interactions except for Fe-C interactions in the C-termination interfaces. Fe-Nb and Fe-Ti covalent bonds are formed in the C-termination interfaces. From the atom charges results listed in Table 5, Fe-C ionic bonds are formed at the C-termination interfaces.

5. Analysis of wear resistances tendency

The wear resistance of coating has been improved after Ti addition, and Ti-1 coating shows the best wear resistance. To achieve a better understand of this tendency, the size and amount of carbide, hardness, wear loss and C content (without the part that carbide used) were summarized, which are shown in Fig. 12. From it, the size of primary carbide and the hardness of coatings show the same tendency with wear resistance tendency in Ti-1, Ti-2 and Ti-3 coating, which means that these two factors are the main reason for the increase of wear loss in Ti- 2 and Ti-3 coating. From the calculated results, the interfacial combination has been improved after Ti addition, which indicates that the combination of carbide and Fe matrix in Ti-1 coating is better than that in Ti-0 coating which will help to prevent the loose of carbide in Ti-1 coating, therefore, broken primary carbides have been found in Ti- 1coating. Compared with Ti-0 coating, better combination of carbide and Fe matrix and formation of primary carbide in Ti-1 coating are the main factors for the increase of wear resistance.

6. Conclusion

In this work, the morphology of (Nb,Ti)C carbides, wear resistance of coatings and interfacial structures of (Nb,Ti)C/α-Fe interfaces with different Ti contents were investigated by experiments and simulations. It is hope to find the tendency of wear resistance influenced factors affected by Ti contents, which are of guiding significance in the (Nb,Ti)C reinforced coatings. The obtained conclusions are as following. a) The amount of carbide is increased and size of carbides is decreased with the increase of Ti content. The average diameter of primary carbide in the Ti-1, Ti-2 and Ti-3 coatings are about 3.2 μm, 2.3 μm and 1.7 μm, respectively. The average amount of primary carbide in the coatings is about 0.35, 0.48 and 0.53 μm^{-2}, respectively. b) The wear weightlessness of Ti-1 coating is the lowest, which is 0.47 $g/N * cm2$. The wear weightlessness of Ti-2 and Ti-3 coatings are increased with the increase of Ti content, however, they are significantly lower than that of Ti-0 coating. c) The stability the interfaces can be improved by element Ti. The stability order of Fe/α-(Nb,Ti)C interfaces is as following: CNb- Fe < NbC-Fe < CTiNb-Fe < CNbTi-Fe < NbTiC-Fe < TiNbCFe. Besides, the

distances of metal atoms at the C-termination interfaces are closed to that at the M-termination interfaces. d) In M-termination surface, weak Fe-M covalent bond is formed at the interface. In C-termination surface, strong FeeC and M-C covalent bond can be observed at the interface, besides, FeeC ionic bonds are also formed.

Acknowledgement
The authors would like to express their gratitude for projects supported by the National Natural Science Foundation of China (No. 51771167 and No. 51705447), Natural Science Foundation of Hebei Province of China (E2017209180) and the Royal Society International Exchange Program.

References
[1] S. Yang, W. Liu, M. Zhong, Z. Wang, TiC reinforced composite coating produced by powder feeding laser cladding, Mater. Lett. 58 (2004) 2958–2962.
[2] R. Colaço, R. Vilar, Laser rapid-alloy prototyping for the development of wear resistant Fe–Cr–C/NbC composite materials, Journal of Laser Applications 15 (2003) 267–272.
[3] J. Jung, S. Kang, Sintered (Ti,W)C carbides, Scr. Mater. 56 (2007) 561–564.
[4] X.H, Wang, F. Han, S.Y. Qu, Z.D, Zou, Microstructure of the Fe-based hardfacing layers reinforced by TiC-VC-Mo2C particles, Surface & Coatings Technology, 202 (2008) 1502–1509.
[5] M. Li, J. Huang, Y.Y. Zhu, Z.G. Li, Effect of heat input on the microstructure of insitu synthesized TiN–TiB/Ti based composite coating by laser cladding, Surf. Coat. Technol. 206 (2012) 4021–4026.
[6] J.H. Jang, C.H. Lee, Y.U. Heo, D.W. Suh, Stability of (Ti,M)C (M=Nb, V, Mo and W) carbide in steels using first-principles calculations, Acta Mater. 60 (2012) 208–217.
[7] Q. Li, Y. Lei, H. Fu, Growth mechanism, distribution characteristics and reinforcing behavior of (Ti, Nb)C particle in laser cladded Fe-based composite coating, Appl. Surf. Sci. 316 (2014) 610–616.
[8] C. Zhao, Y. Zhou, X. Xing, S. Liu, X. Ren, Q. Yang, Precipitation stability and microproperty of (Nb, Ti)C carbides in MMC coating, J. Alloys Compd. 763 (2018) 670–678.
[9] C. Zhao, X. Xing, J. Guo, Z. Shi, Y. Zhou, X. Ren, Q. Yang, Micro-properties of (Nb,M)C carbide (M= V, Mo, W and Cr) and precipitation behavior of (Nb,V)C in carbide reinforced coating, J. Alloys Compd. 788 (2019) 852–860.
[10] L. Zhong, F. Ye, Y. Xu, J. Li, Microstructure and abrasive wear characteristics of in situ vanadium carbide particulate-reinforced iron matrix composites, Materials & Design (1980–2015) 54 (2014) 564–569.
[11] S. Wei, J. Zhu, L. Xu, L. Rui, Effects of carbon on microstructures and properties of high vanadium high-speed steel, Mater. Des. 27 (2006) 58–63.
[12] H. Cao, X. Dong, S. Chen, M. Dutka, Y. Pei, Microstructure evolutions of graded high-vanadium tool steel composite coating in-situ fabricated via atmospheric plasma beam alloying, J. Alloys Compd. 720 (2017) 169–181.
[13] J.W. Park, C.L. Huo, S. Lee, Composition, microstructure, hardness, and wear properties of high-speed steel rolls, Metallurgical & Materials Transactions A 30 (1999) 399–409.
[14] T. Gong, P. Yao, X. Zuo, Z. Zhang, Y. Xiao, L. Zhao, H. Zhou, M. Deng, Q. Wang, A. Zhong, Influence of WC carbide particle size on the microstructure and abrasive wear behavior of WC–10Co–4Cr coatings for aircraft landing gear, Wear 362-363 (2016) 135–145.
[15] H. Sawada, S. Taniguchi, K. Kawakami, T. Ozaki, First-principles study of interface structure and energy of Fe/NbC, Model. Simul. Mater. Sci. Eng. 21 (2013) 045012.

[16] J.C. Li, H.Q. Song, J.W. Wang, J. Shen, Atomic study of semi-coherent interfacial structure at Fe[110]/TMC[001] (TM=V, Nb and Ta) interfaces, Adv. Mater. Res. 1081 (2014) 232–236.
[17] A. Arya, E.A. Carter, Erratum: structure, bonding, and adhesion at the TiC(100)/Fe (110) interface from first principles [J. Chem. Phys. 118, 8982 (2003)], J. Chem. Phys. 120 (2004) 1142.
[18] J. Yang, P. Zhang, Y. Zhou, J. Guo, X. Ren, Y. Yang, Q. Yang, First-principles study on ferrite/TiC heterogeneous nucleation interface, Journal of Alloys & Compounds 556 (2013) 160–166.
[19] X. Fan, B. Chen, M. Zhang, D. Li, Z. Liu, C. Xiao, First-principles calculations on bonding characteristic and electronic property of TiC (111)/TiN (111) interface, Mater. Des. 112 (2016) 282–289.
[20] Y. Wang, N. Chen, Atomistic investigations of misfit dislocation for Pt/SiC(111) interface fracture, Model. Simul. Mater. Sci. Eng. 18 (2010) 065012.
[21] J. Yang, Z. Ye, J. Huang, S. Chen, Y. Zhao, First-principles calculations on wetting interface between Ag-Cu-Ti filler metal and SiC ceramic: Ag (1 1 1)/SiC (1 1 1) interface and Ag (1 1 1)/TiC (1 1 1) interface, Appl. Surf. Sci. 462 (2018) 55–64.
[22] X. Yun, Y.F. Zhou, B. Zhao, X.L. Xing, J. Yang, Y.L. Yang, Q.X. Yang, Influence of Nano-Y2O3 on Wear resistance of hypereutectic Fe–Cr–C Hardfacing coating, Tribol. Lett. 58 (2015) 23.
[23] W. Kohn, L.J. Sham, Self-consistent equations including exchange and correlation effects, Phys. Rev. 140 (1965) A1133–A1138.
[24] W. Kohn, L.J. Sham, Quantum density oscillations in an inhomogeneous electron gas, Phys. Rev. 137 (1965) 1697–1705.
[25] D. Vanderbilt, Soft self-consistent pseudopotentials in a generalized eigenvalue formalism, Phys. Rev. B 41 (1990) 7892–7895.
[26] J.P. Perdew, E.R. McMullen, A. Zunger, Density-functional theory of the correlation energy in atoms and ions: a simple analytic model and a challenge, Phys. Rev. A 23 (1981) 2785–2789.
[27] D.J. Chadi, Special points for Brillouin-zone integrations, Physical Review B Condensed Matter 16 (1977) 5188–5192.
[28] C.G. Broyden, The convergence of a class of double rank minimization algorithms II, The New Algorithm, 1970.
[29] C. Zhao, Y. Zhou, X. Xing, S. Liu, X. Ren, Q. Yang, Investigation on the relationship between NbC and wear-resistance of Fe matrix composite coatings with different C contents, Appl. Surf. Sci. 439 (2018) 468–474.
[30] Y. Yan, B. Wei, F.U. Zhengyi, H. Lin, R. Yuan, In situ TiC particulates reinforced ferrous matrix composite and its microstructure forming mechanism, Acta Metallrugica Sinica 35 (1999) 1117–1120.
[31] X. Cai, Y. Xu, N. Zhao, L. Zhong, Z. Zhao, J. Wang, Investigation of the adhesion strength and deformation behaviour of in situ fabricated NbC coatings by scratch testing, Surf. Coat. Technol. 299 (2016) 135–142.
[32] M. Charleux, W.J. Poole, M. Militzer, A. Deschamps, Precipitation behavior and its effect on strengthening of an HSLA-Nb/Ti steel, Metallurgical & Materials Transactions A 32 (2001) 1635–1647.
[33] L.M. Liu, S.Q. Wang, H.Q. Ye, First-principles study of polar Al/TiN(1 1 1) interfaces, Acta Mater. 52 (2004) 3681–3688.
[34] T.D. Kühne, T.A. Pascal, E. Kaxiras, Y. Jung, New insights into the structure of the vapor/water Interface from large-scale first-principles simulations, J. Phys. Chem. Lett. 2 (2011) 105.

No.	C	Nb	Cr	Mn	Si	V	Ti	Fe
Ti-0	1.15	4.48	5.43	1.20	1.35	0.51	–	Bal.
Ti-1	1.13	4.40	5.34	1.32	1.27	0.46	0.15	Bal.
Ti-2	1.20	4.38	5.27	1.23	1.23	0.45	0.32	Bal.
Ti-3	1.17	4.31	5.25	1.26	1.33	0.50	0.41	Bal.

Table 1 Compositions of coatings (wt%).

Chemical element	Primary carbide		Eutectic carbide	
	Weight percentage	Atom percentage	Weight percentage	Atom percentage
Ti	15.29	10.78	3.14	2.19
Nb	54.74	19.89	34.96	12.59
Fe	3.95	2.39	35.40	21.22
Cr	0.86	0.56	3.14	2.02
V	1.38	0.91	0.58	0.38
C	22.90	64.37	21.78	60.70

Table 2 EDS analysis results of primary and eutectic carbide.

Interface	CNb-Fe	CNbTi-Fe	CTiNb-Fe	NbC-Fe	NbTiC-Fe	TiNbC-Fe
W_{ad} (J/m^2)	−1.08	1.36	0.67	0.11	2.91	3.17
d_0 (Å)	2.88	2.93	2.89	1.86	1.87	1.85
d_1 (Å)	3.55	3.57	3.51	2.86	2.91	2.90

Table 3 Adhesion work (J/m2) and interface distance (Å).

Interface	CNb-Fe (Fe–Nb)	CNbTi-Fe (Fe–Nb) (Fe–Ti)	CTiNb-Fe (Fe–Nb)	NbC-Fe (Fe–C) (Fe–Nb)	NbTiC-Fe (Fe–C) (Fe–Nb) (Fe–Ti)	TiNbC-Fe (Fe-C(Nb)) (Fe-C(Ti)) (Fe-Nb(Nb)) (Fe-Nb(Ti))
Bond populations	−0.11	−0.04 0.08	0.05	0.21 0.27	0.39 0.02 0.21	0.32 0.30 0.12 0.10

Table 4 Calculated Mulliken overlap population (MOP): bond population.

Interface	CNb-Fe	CNbTi-Fe	CTiNb-Fe	NbC-Fe	NbTiC-Fe	TiNbC-Fe
	Fe	Fe(Nb)	Fe	Fe	Fe	Fe
	Nb	Fe(Ti)	Nb	Nb	Nb	Nb
		Nb		C	Ti	C
		Ti			C	
Atom charges	0.13	0.14	0.16	0.15	0.10	0.14
	0.54	0.11	0.52	0.63	0.57	0.59
		0.50		−0.73	0.75	−0.74
		0.71			−0.73	

Table 5 Calculated Mulliken overlap population (MOP): Atom charges (e).

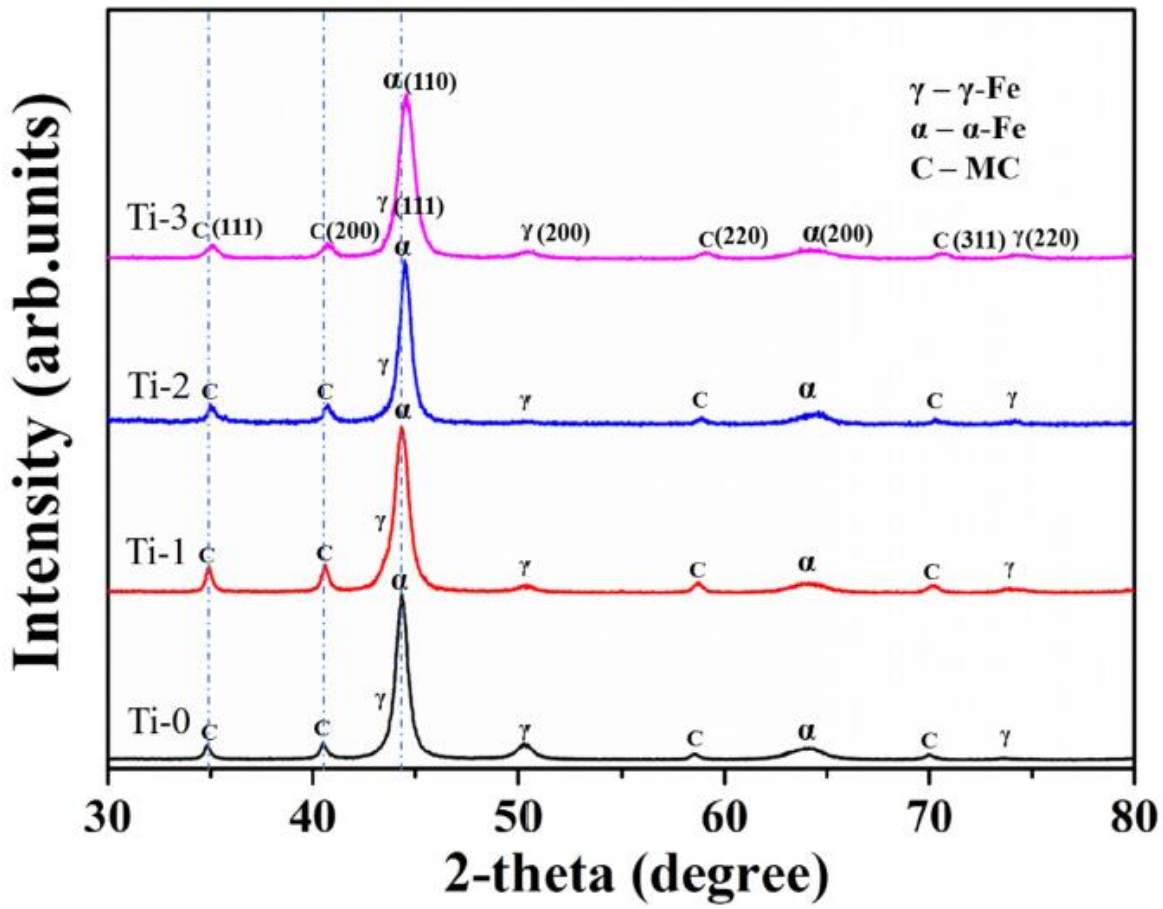

Fig. 1. XRD results of coatings with different Ti contents.

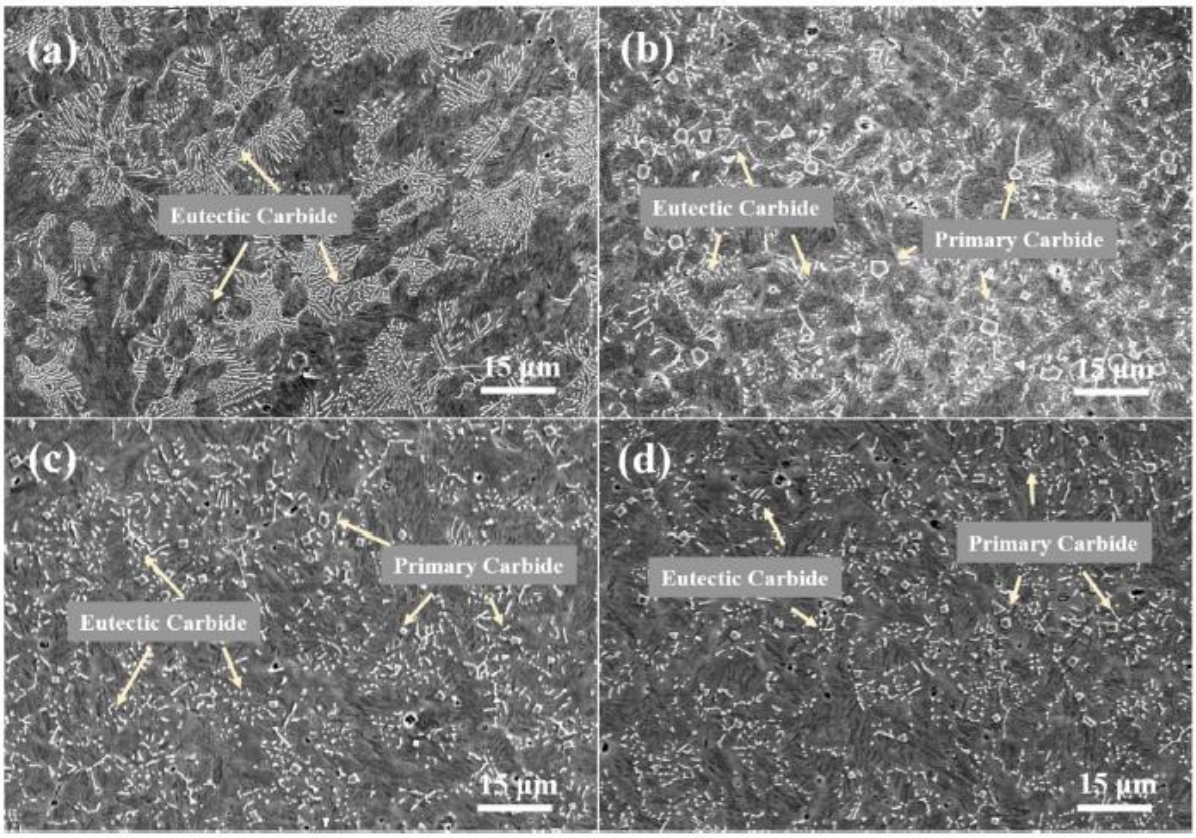

Fig. 2. SEM images of the coatings: (a) Ti-0 (b) Ti-1 (c) Ti-2 (d) Ti-3.

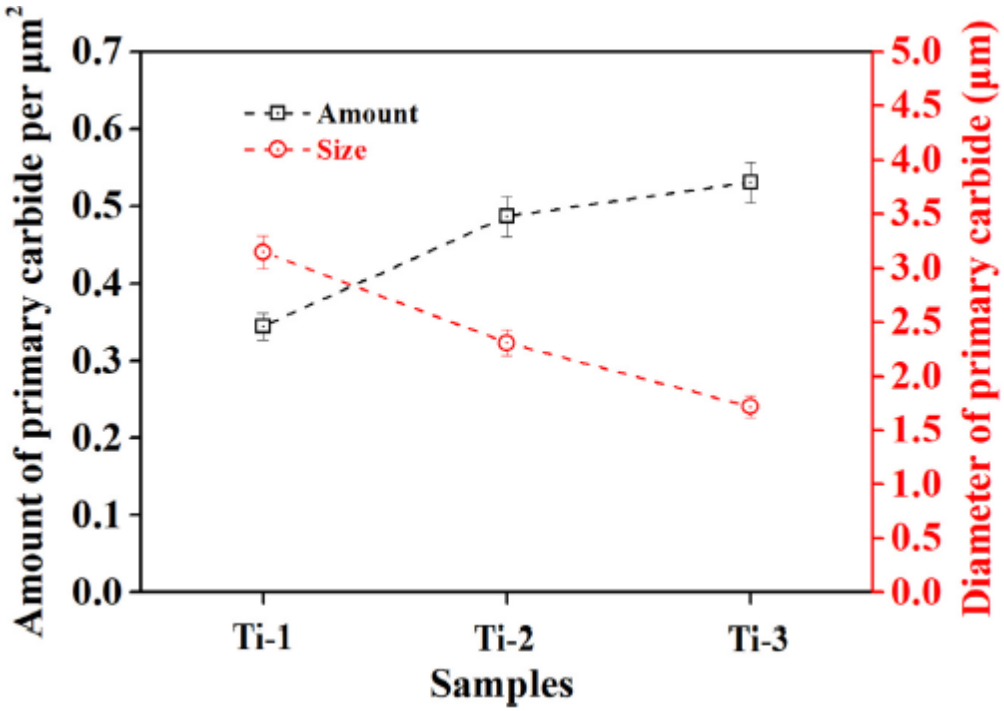

Fig. 3. Amount and size of primary carbide in Ti-1, Ti-2 and Ti-3 coatings.

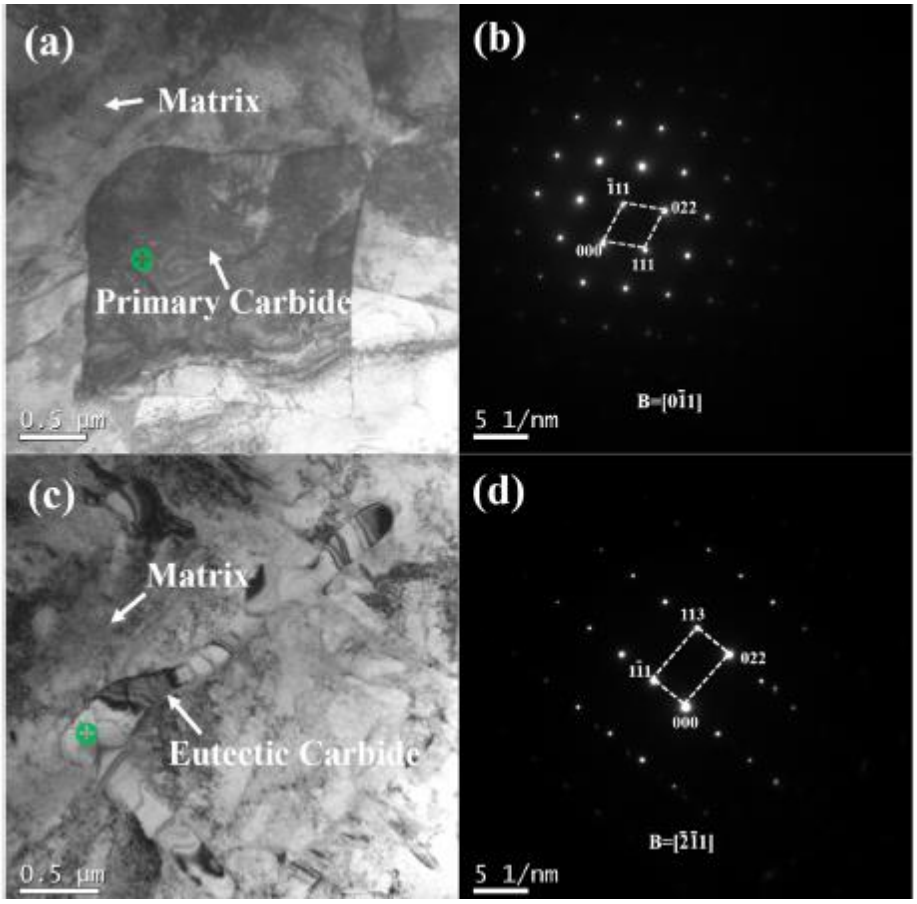

Fig. 4. TEM image of primary and eutectic carbide and SEAD pattern of carbides: (a) primary carbide (b) SEAD pattern of primary carbide (c) eutectic carbide (d) SEAD pattern of eutectic carbide.

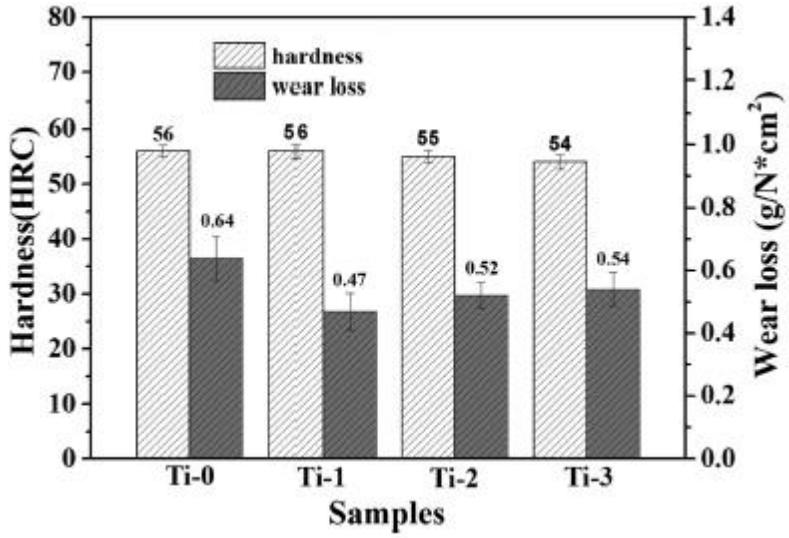

Fig. 5. Hardness and wear weightlessness of the coatings.

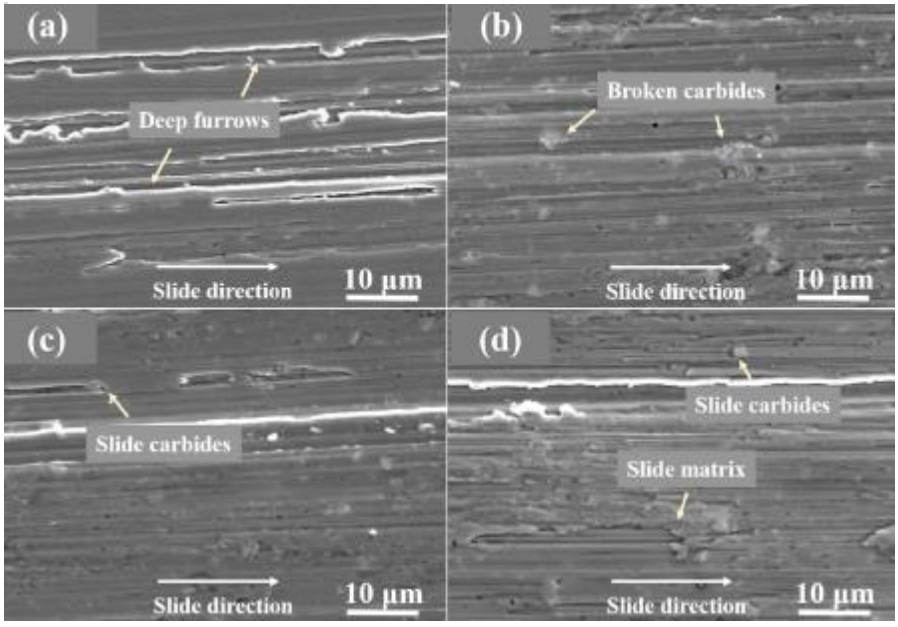

Fig. 6. Worn surfaces morphology of the coatings: (a) Ti-0 (b) Ti-1 (c) Ti-2 (d) Ti-3.

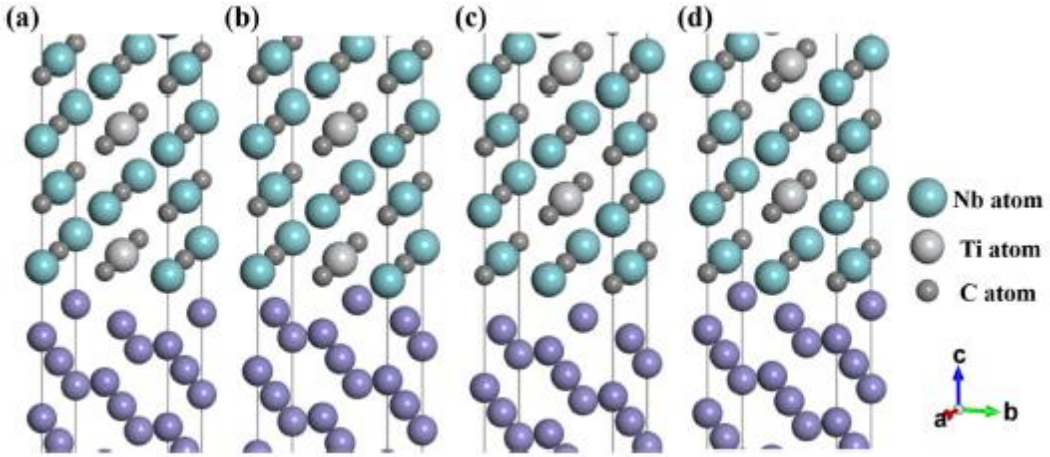

Fig. 7. Interface models of (Nb,Ti)C with α-Fe: (a) CNbTi-Fe (b) NbTiC-Fe (c) CTiNb-Fe (d) TiNbC-Fe.

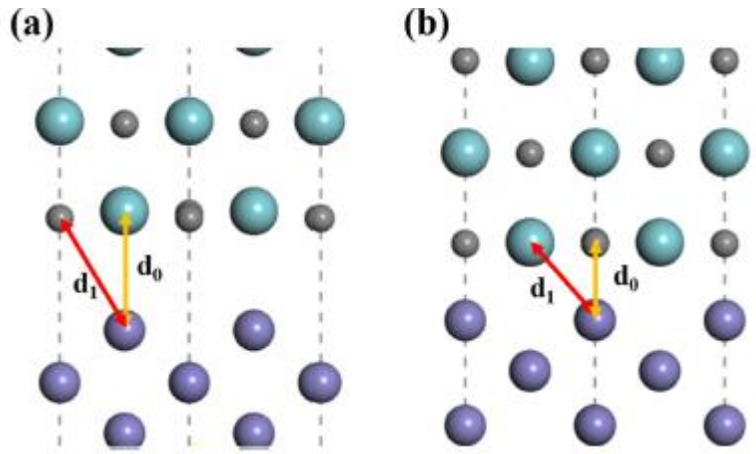

Fig. 8. Interface distance of M-termination (metal atoms above the Fe atoms) and C-termination (carbon atoms above the Fe atoms) interfaces: (a) M-termination (b)C-termination.

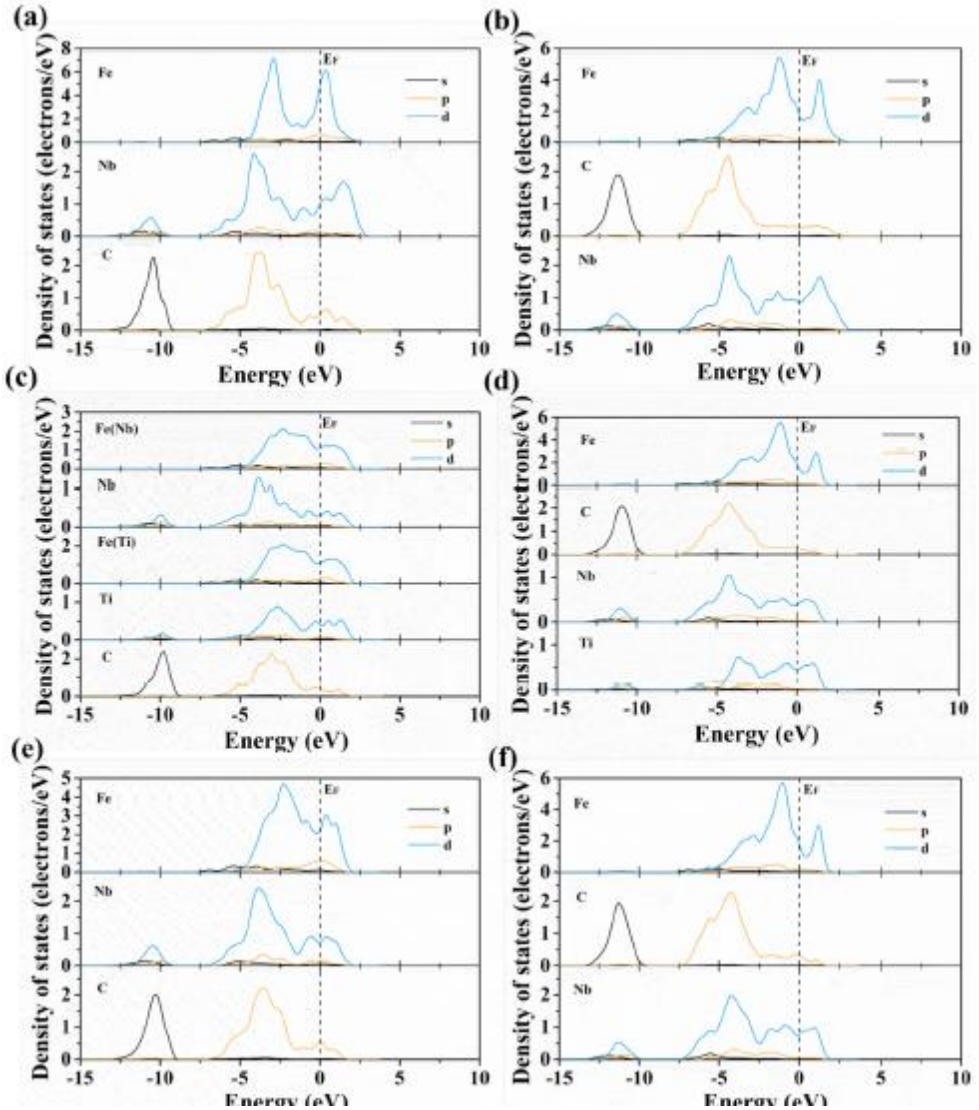

Fig. 9. PDOS of the interface models: (a) CNb-Fe (b) NbC-Fe (c) CNbTi-Fe (d) NbTiC-Fe (e) CTiNb-Fe (f) TiNbC-Fe.

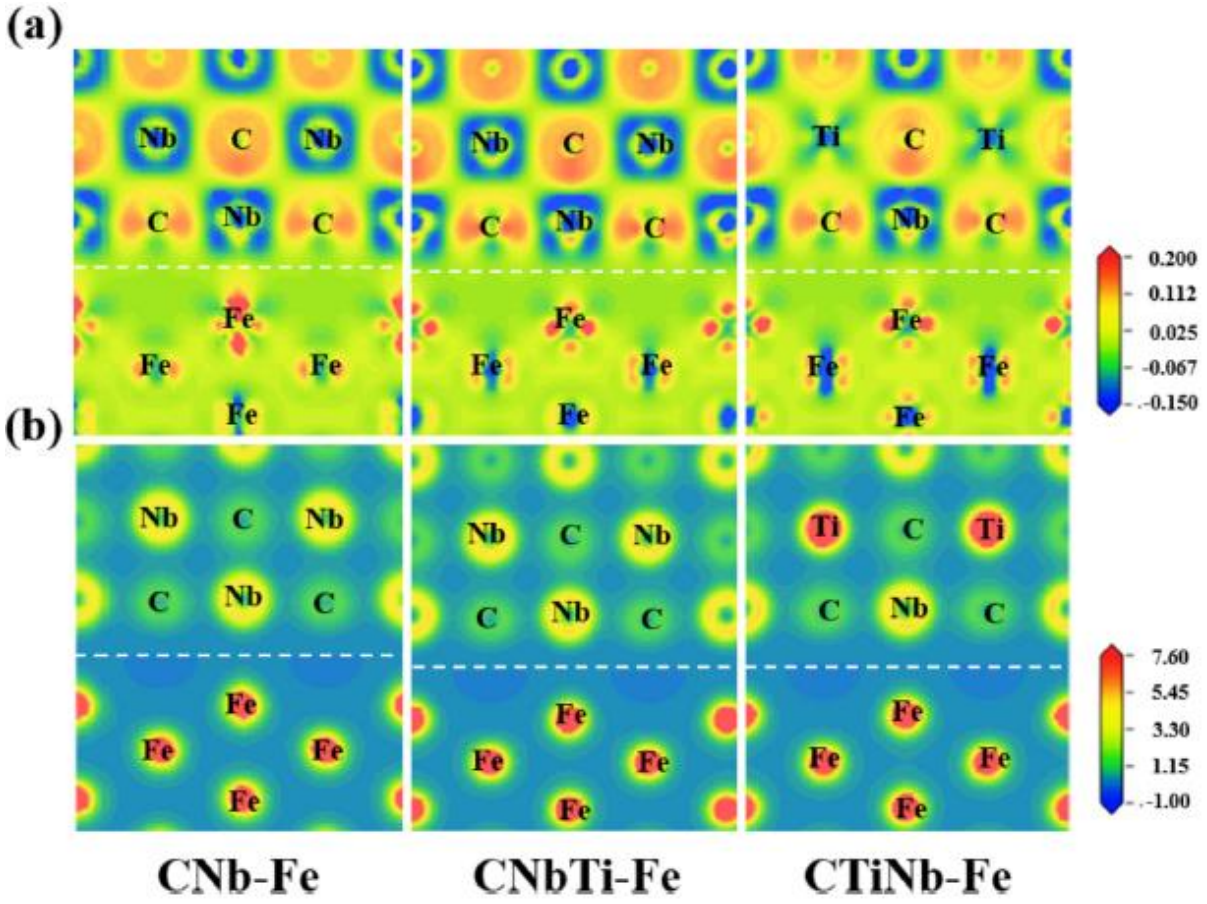

Fig. 10. Charge density and charge density difference of M-termination interfaces: (a) charge density difference and (b) charge density.

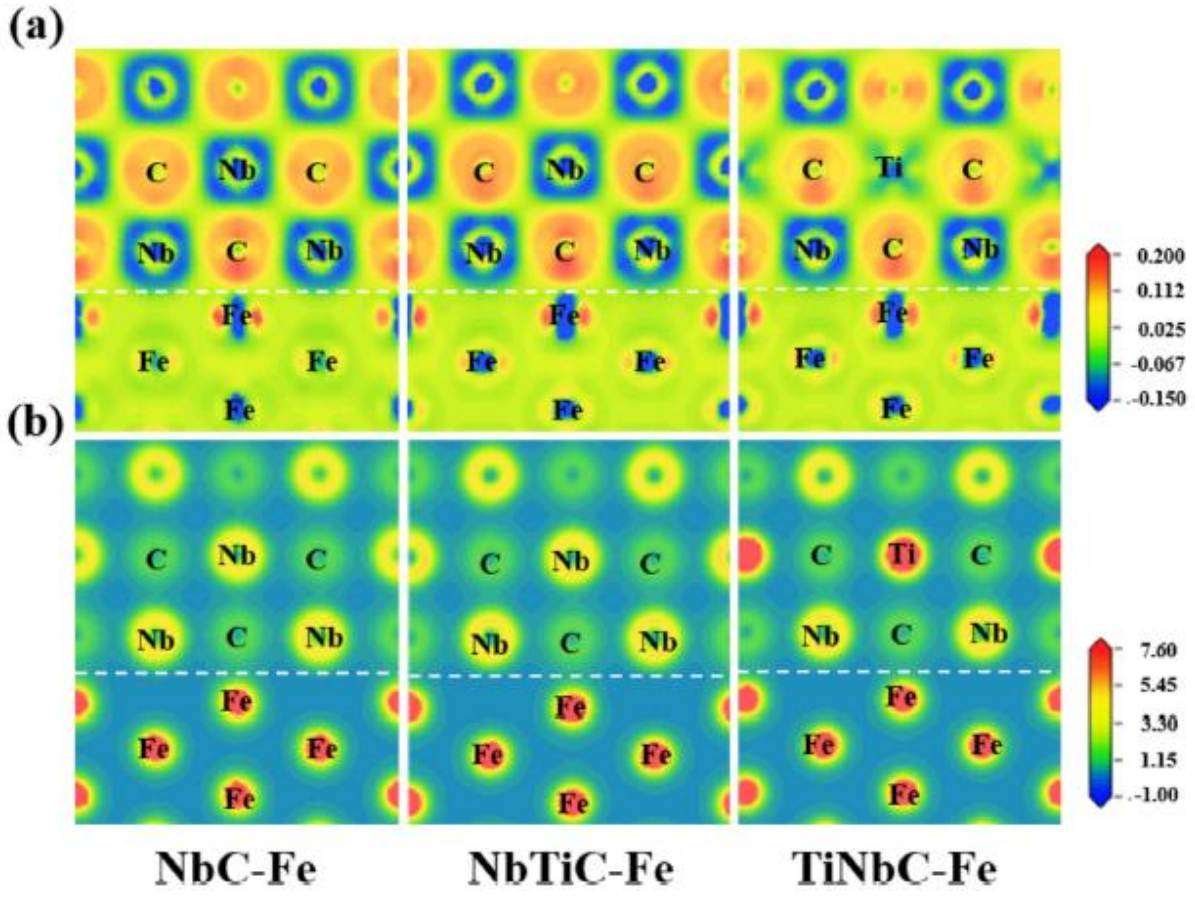

Fig. 11. Charge density and charge density difference of C-termination interfaces: (a) charge density difference and (b) charge density.

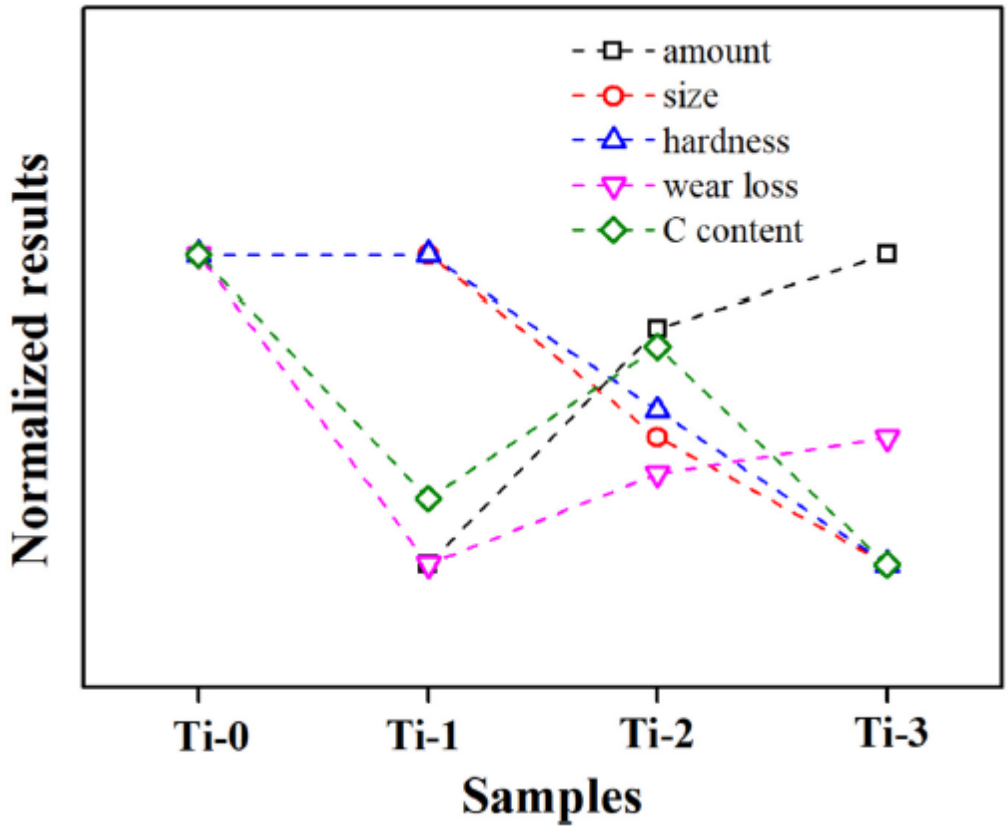

Fig. 12. Summary of the size and amount of carbide, hardness, wear loss and C content of the coatings.